INDERSCIENCE PUBLISHERS
Linking academia, business and industry through research

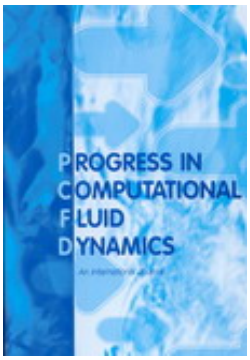


**Progress in Computational Fluid Dynamics, An International Journal**

ISSN online: 1741-5233 - ISSN print: 1468-4349
https://www.inderscience.com/pcfd

# Modelling and simulation of ash accumulation in SP boiler of decomposition kiln

Shunsheng Xu, Chong Shen, Kongyao Wang, Fulian Yao, Jiazhen He

**DOI:** 10.1504/PCFD.2023.10053764

**Article History:**

| | |
|---|---|
| Received: | 26 March 2021 |
| Last revised: | 10 December 2021 |
| Accepted: | 15 February 2022 |
| Published online: | 02 February 2023 |

# Modelling and simulation of ash accumulation in SP boiler of decomposition kiln

Shunsheng Xu

School of Mechanical Engineering,
Xiangtan University,
Xiangtan 411105, China
and
School of Energy Science and Engineering,
Central South University,
Changsha 410083, China
Email: 787749816@qq.com

Chong Shen*, Kongyao Wang,
Fulian Yao and Jiazhen He

School of Mechanical Engineering,
Xiangtan University,
Xiangtan 411105, China
Email: 709184918@qq.com
Email: 1092175631@qq.com
Email: 3190025871@qq.com
Email: 1356088529@qq.com
*Corresponding author

**Abstract:** In this paper, the problem of ash accumulation in the superheater of a suspension preheater (SP) waste heat boiler is studied. A comprehensive ash accumulation growth model, including deposition and removal process, is established and verified by experimental results. According to the established model, the effects of flue gas velocity, ash concentration and tube shape on the ash accumulation are studied. The ash growth prediction model based on the initial simulation value fitting is proposed and used in the research of ash prediction. The results show that the ash growth prediction model can predict the ash accumulation better; the ash accumulation rate increases with the flue gas velocity and the ash concentration; the ash accumulation time constant decreases; the maximum ash accumulation decreases negatively with the flue gas velocity but is little affected by the ash concentration; the performance of the oval tube to reduce the ash accumulation is better than that of the round tube; when the oval tube layout angle is 45°, the effect is best; and the comprehensive evaluation effect on the heat transfer and resistance is the best.

**Keywords:** SP waste heat boiler; ash accumulation; the simulation; accumulation of ash growth prediction; oval tube layout angle.

**Reference** to this paper should be made as follows: Xu, S., Shen, C., Wang, K., Yao, F. and He, J. (2023) 'Modelling and simulation of ash accumulation in SP boiler of decomposition kiln', *Progress in Computational Fluid Dynamics*, Vol. 23, No. 1, pp.52–63.

**Biographical notes:** Shunsheng Xu graduated with a Master's in Thermal Energy Engineering and an Associate Professor and Master Supervisor. He has been engaged in scientific research and teaching in the field of power engineering and engineering thermophysics for nearly 30 years. He has presided over more than 20 scientific research projects commissioned by enterprises and participated in more than ten enterprise scientific research projects mainly led by master and doctoral supervisors.

Chong Shen received his Bachelor's degree from the Xiangtan University and is currently studying for a Master's degree from Xiangtan University. His main research direction is thermal process simulation and optimisation.

Kongyao Wang is currently an outstanding undergraduate majoring in Energy and Power Engineering at the Xiangtan University. He has participated in many academic research projects and won university scholarship and merit student honour for many times.

Fulian Yao is currently an outstanding undergraduate majoring in Energy and Power Engineering at the Xiangtan University. He has won national encouragement scholarship and many university honours.

Jiazhen He received his Master's degree from the School of Mechanical Engineering, Xiangtan University. His main research direction is thermal process simulation and optimisation. He has made some research achievements in the field of engineering thermophysics.

## 1 Introduction

When the cement decomposition kiln is running, a large amount of low-temperature flue gas of about 300°C–400°C is discharged from the kiln head chiller and the kiln tail preheater, and the heat carried by it accounts for 30% of the total energy consumption of the cement firing system (Kong, 2009). Because of its high ash concentration and low temperature, it is difficult to recycle the waste heat of low-temperature flue gas directly. The direct discharge of the low-temperature flue gas will significantly reduce the thermal efficiency of the decomposition furnace and result in serious pollution of the ecological environment (Ren et al., 2014). The efficient utilisation of the waste heat boiler to recover the waste heat is conducive to improving the decomposition kiln's thermal efficiency and the enterprise's economic benefits, which is of great significance to promote energy conservation and emission reduction work (Amiri and Vaseghi, 2015; Zhang et al., 2018).

Ash accumulation is one of the main problems reducing the thermal efficiency of the waste heat boiler (Zhang et al., 2009). The formation of ash is mainly due to inertial particle collision and thermophoretic force (Yang et al., 2017): the large inertia of large particles due to their large mass makes it possible to collide directly through the boundary layer and the heat exchange surface (Zbogar et al., 2009); due to its small mass and low inertia, the smaller particles move to the heat transfer surface only using thermophoretic force or turbulent action of the flue gas (Pérez et al., 2016; Fang et al., 2010; Lin and Tsai, 2003). The high-ash flue gas of the SP waste heat boiler is introduced from the discharge port of the kiln tail preheater. The ash particles are small and easy to deposit on the superheater tube bundle (Gu et al., 2017). This increases the heat transfer resistance, reduces the heat exchange rate between the flue gas and the working medium in the heat exchange tube bundle, and also causing uneven deposition on the tube wall, resulting in uneven heating and high-temperature corrosion, thereby causing a burst tube, etc. (Si and Fan, 2015; Harding and O'Connor, 2007). It is of great significance to study the ash accumulation in the superheater of SP waste heat boiler of the decomposing kiln and try to reduce the ash accumulation to improve the recovery efficiency of waste heat, the economic benefit of enterprises and promote energy conservation and emission reduction.

Some researchers investigated the ash accumulation phenomenon in boilers. Miao et al. (2022) studied the ash deposition characteristics in the pulverised coal reaction at high temperatures and concluded that inertial collision is the main reason for the ash formation. Mu et al. (2021) proposed an elastic-plastic collision deposition model for judging particles and walls by studying the energy conservation in the collision process of particles and walls. Tang et al. (2018) studied the influence of particle incidence angle on deposition, proposed a critical incidence angle model for deposition, and found that particle deposition does not occur when the incidence angle is greater than the critical angle. Based on the Kern-Seaton model, Chen et al. (2004) established Chen Baokang ash growth prediction model and verified the model's reliability through experiments. Ye et al. (2018) studied the characteristics of oval tubes and circular tubes in reducing ash accumulation, showing that the former had a better effect in reducing ash accumulation than the latter. However, there is no report on studying a more realistic comprehensive model of ash accumulation growth that includes deposition and removal processes. Oval angle greatly influences ash accumulation and heat transfer of heat exchangers, but there is no in-depth systematic research report.

Although a lot of fruitful work has been done on the study of airflow ash deposition, there are few reports on the modelling and simulation of the comprehensive ash accumulation growth model, which contains deposition, rebound and stripping. To improve the reliability of the simulation model of ash deposition, this paper carries out the modelling and simulation research of the comprehensive ash accumulation growth model and uses fluent software suitable for particle phase flow research as a simulation research platform. The research contents are as follows:

1 A comprehensive model of ash accumulation, including ash deposition and removal process, is established. The simulation program based on this model is compiled based on fluent software, UDF macro and C Programming language function library.

2 Based on the comprehensive ash accumulation growth model, the effect of FG velocity, ash concentration and layout angle of oval heat transfer tube on ash accumulation is studied. Based on the fitting of the first 120s simulation results, a prediction model of ash accumulation growth is established. The influence rule of the velocity of flue gas, ash concentration in flue gas and layout angle of the oval tube on the characteristics of ash accumulation time is studied through the prediction model.

3 Optimisation study of the layout angle of the oval tube.

The above research will help researchers (or plant operators) understand the characteristics of ash

accumulation under various conditions. Provide theoretical basis and technical support for SP waste heat boiler design and economical operation.

## 2 Model description

### 2.1 The basic assumptions

To simplify the modelling and save simulation time, the following reasonable assumptions are made based on the actual ash accumulation of the SP waste heat boiler superheater.

1 The superheater is simplified to a four heat exchange tube model due to the symmetric structure and its internal widget structure is ignored.

2 Only consider the impact of flue gas flow on the movement of particles.

3 The shape of the ash particles is ignored, and the particles are assumed to be equal diameter pellets. Because the volume concentration is very low, the interparticle force is neglected.

4 Because this paper mainly studies particles' collision, deposition and removal, the chemical reaction between ash particles and heat exchange tube is ignored.

### 2.2 Comprehensive ash accumulation growth model

The deposition process of ash particles on the tube wall of the superheater of the SP waste heat boiler can be described as: the ash particles in the flue gas collide with the tube wall, part of which adheres to the tube wall to form ash accumulation; part of it re-enters the flue gas due to bounce; One part collides with the accumulated ash deposited on the tube wall, causing some of the deposited particles to peel off from the ash layer and re-enter the flue gas. Based on the above ash accumulation process, the influence of adhesion deposition, particle rebound, and peeling and removal of deposited ash particles should be considered when establishing the ash accumulation model. In conclusion, this paper establishes a comprehensive ash accumulation growth model that includes the three influencing factors.

When the flue gas entering the superheater exchanges heat with the heat exchange tube bundle, the particles in the flue gas also randomly collide with the heat exchanger tube bundle (mostly oblique collision) and deposit on the tube bundle. The collision process between the ash particles and the wall of the heat exchange tube and the ash layer on the tube wall is shown in Figure 1: $V_i$ is the incident velocity when particles collide, m/s; $V_t$ is the particle escape velocity after collision, m/s; $V_{it}$ is the tangential velocity of particle collision, m/s; $V_{in}$ is the normal velocity of particle collision, m/s; $\theta'$ is the angle of incidence.

The critical incident angle of the incident particle is studied, that is, whether the tangential component of the collision contact force when the incident particle collides with the wall surface of the heat exchange tube is greater than or equal to the adhesion force between the incident particle and the ash layer on the wall surface. According to contact mechanics (Johnson, 1985) and Newton's theorem, the force calculation formula of incident particles is obtained, as shown in equation (1):

$$F_t = k_t V_{it} \Delta t \geq \mu^* F_{adh} = \mu^* 3\pi R^* \Gamma \tag{1}$$

where $F_t$ is the tangential component of the collision contact force received by the particle, $N$; $k_t$ is tangential stiffness (Mindlin, 1949), N/m; $\Delta t$ is collision contact time, $s$; $\mu^*$ is the effective friction coefficient (Abd-Elhady et al., 2006), Pa·s; $F_{adh}$ is the adhesion between particles and sedimentary body, N; $\Gamma$ is the surface energy between contact bodies, J; $R^*$ is the effective contact radius, $m$, and its calculation formula is shown in equation (2):

$$1/R^* = 1/R_1 + 1/R_2 \tag{2}$$

where $R_1$ $R_2$ are impact particles and deposition body radii respectively, $m$.

**Figure 1** Material particle impact wall process

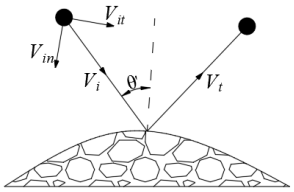


The tangential impact energy of the incident particle $Q_{it}$ is:

$$Q_{it} = \frac{1}{2} k_t \left(V_{it} \Delta t\right)^2 = \frac{1}{2} \mu^{*2} F_{adh}^2 / k_t \tag{3}$$

Tangential stiffness $k_t$ (Mindlin, 1949) is approximately shown in equation (4):

$$k_t \approx 8 G^* a \tag{4}$$

In equation (4), $G^*$ is the effective shear modulus between two colliding bodies, Pa.

In terms of energy, the normal impact energy of the incident particle is approximately equal to the adhesion energy between the incident particle and the deposited body when the particle and the surface break away. The calculation formula is as follows:

$$Q_{in} = \frac{1}{2} k_i \left(V_{in} \Delta t\right)^2 \approx Q'_A = 2\pi a^2 \Gamma \tag{5}$$

In equation (5), $Q'_A$ is the adhesion energy between particles and sedimentary body, J. $a$ is the radius of the contact surface, m, and the calculation formula is shown in equation (6):

$$a = \beta a_0 \tag{6}$$

In equation (6), $a_0$ is the initial contact surface radius (Thornton and Ning, 1998) only affected by adhesive force $F_{adh}$ between contact surfaces, N. $\beta$ is the effective coefficient of contact surface radius, and $a_0$ is shown in equation (7):

$$a_0 = \left(9\pi\Gamma R^{*2}/E^*\right)^{1/3} \tag{7}$$

In equation (7), $E^*$ is the effective young's elastic modulus between two colliding bodies, Pa, and its definition is shown in equation (8):

$$1/E^* = \left(1-v_1^2\right)/E_1 + \left(1-v_2^2\right)/E_2 \tag{8}$$

In equation (8), $v_1$ and $v_2$ are the Poisson ratios of particles and sedimentary bodies respectively, and the values are 0.27. $E_1$ and $E_2$ are young's modulus of particles and sedimentary bodies respectively, with values of $1.17 \times 10^{49}$ *Pa* and $4.92 \times 10^{10}$ *Pa*.

Equation (9) can be obtained from Figure 1 and the relationship between velocity and kinetic energy:

$$\tan\theta_{ca} = v_{it}/v_{in} = \left(Q_{it}/Q_{in}\right)^{1/2} \tag{9}$$

Simultaneous equations (1), (2), (3), (4), (5) and (9) can be obtained as follows:

$$\mu^*/(32\beta^3)^{1/2} \tag{10}$$

In equation (10), $\theta_{ca}$ is the critical incident angle of the particle (Tang et al., 2018).

It is easy to deduce that when the incident particle collides with the wall when its elastic energy storage is greater than or equal to the adhesion energy between the particle and the wall ash layer, the incident particle will rebound. According to the law of energy conservation, the energy equation of particle collision process equation (11) can be obtained (Han et al., 2014).

$$\frac{1}{2}mV_i^2 + Q_A = Q_e + Q_p \tag{11}$$

In equation (11), $Q_A$ is the adhesion energy between the impact particles and the surface of the sedimentary body, J; $Q_e$ is elastic energy storage caused by elastic deformation of particles, J; $Q_p$ is the energy loss caused by plastic deformation of particles, J.

When the incident particles bounce off the wall surface, equation (12) can be obtained according to the energy conservation law.

$$\frac{1}{2}mV_t^2 = Q_e - Q'_A \tag{12}$$

In equation (12), $m$ is the mass of incident particles, kg.

When particles collide with the wall surface and bounce away, the calculation formula for the relative approach $\alpha_f$ (Thornton and Ning, 1998) of the bounce is shown in equation (13).

$$\alpha_f = \left[3P_c^2\left(16R^*E^{*2}\right)^{-1}\right]^{1/3} \tag{13}$$

In equation (13), $P_c$ is the pressure on the wall surface when the particles rebound, it is as follows:

$$P_c = \frac{3}{2}\pi\Gamma R^* \tag{14}$$

Johnson et al. (1971) pointed out that when the particles bounce off the wall after the collision, the wall surface needs to do extra work $W_s$ on the particles to ensure the separation of the particles from the wall surface, J. The work is shown in equation (15).

$$W_s = P_c a_f = 7.58\left(\Gamma^5 R^{*4} E^{*-2}\right)^{1/3} \tag{15}$$

If the energy loss caused by the plastic deformation of the particles is ignored, the dissipative work of the particles in rebound is equal to the work done by the wall on the particles, and equation (16) can be obtained.

$$\frac{1}{2}mV_i^2 - \frac{1}{2}mV_t^2 = W_s \tag{16}$$

When the particle detachment velocity $V_t$ is equal to zero, the incident velocity $V_i$ at this time is the critical rebound velocity $V_s$, m/s (Mu et al., 2021). From equation (15) and equation (16), the critical rebound speedometer expression equation (17) can be obtained.

$$V_s = 1.84\left[(\Gamma/R)^5 \rho^{-3} E^{*-2}\right]^{1/6} \tag{17}$$

According to the Hertz theory (Johnson, 1985), the two-particle collision contact point normal force $P$ is as in equation (18):

$$P = \frac{4}{3}E^* R^{*1/2}\alpha 3/2 \tag{18}$$

In equation (18), $\alpha$ is the relative approach of the two-particle, determined by the contact radius $\alpha$ of the two particles:

$$\alpha = a^2 / R^* \tag{19}$$

According to the JKR theory (Johnson et al., 1971), the normal contact radius of the particle collision point is calculated as equation (20):

$$a = \left[3PR^*\left(4E^*\right)^{-1}\right]^{1/3} \tag{20}$$

The incident particle velocity defining the detachment of the deposited particles on the wall surface is defined as the critical stripping velocity $V_y$, m/s (Mu et al., 2021). The peeling speed calculation equation (21) is obtained from equation (18) and equation (19):

$$\frac{1}{2}m^* V_y^{\,2} = \int_0^{\alpha_f} P d\alpha = \frac{8E^* a_y^5}{15R^{*2}} \tag{21}$$

In equation (21), $m^*$ for effective collision quality, mg, the formula is as shown in equation (22):

$$1/m^* = 1/m_1 + 1/m_2 \tag{22}$$

In equation (22), $m_1$ and $m_2$ are the masses of incident particles and deposited particles on the wall respectively, mg.

The Hertz pressure between the two colliding particles (Johnson, 1985) is calculated as equation (23):

$$p = 3P / 2\pi a^2 \tag{23}$$

When the ultimate pressure $p_y$ is defined as particle contact radius $a_y$, equation (24) for calculating the ultimate pressure is obtained from equation (20) and equation (23):

$$p_{\mathrm{y}} = 2E^* a_{\mathrm{y}} (\pi R^*)^{-1} \tag{24}$$

The particle density changes very little with the pressure and is regarded as a constant. Combining equation (21) and equation (24), equation (25) can be used to calculate the critical stripping speed:

$$V_{\mathrm{y}} = 1.56\left[ p_{\mathrm{y}} \left(E^{*4}\rho\right)^{-1} \right]^{1/2} \tag{25}$$

In summary, the judgement criteria of the comprehensive growth model of ash accumulation can be obtained as follows:

1 When the incident angle of ash particles is greater than the critical incident angle, no accumulation of ash.

2 When the incident angle of ash particles is smaller than the critical incident angle is:
   - The incident velocity of the ash particles is smaller than critical rebound speed, resulting in ash accumulation.
   - When the incident velocity of the ash particles is greater than critical rebound speed and less than critical peeling speed, the ash particles collide with the heat exchange tube wall surface and bounce into the flue gas stream.
   - When the incident velocity of the ash particles is greater than the critical peeling speed, part of the accumulated ash particles deposited on the heat exchange tube bundle is peeled off, and the deposition amount is reduced.

## 2.3 Computational domain

This paper mainly studies the influence of flue gas velocity and ash concentration on ash accumulation. Based on the aforementioned assumptions and simplifications of the superheater, a three-dimensional four-tube geometric model is established to study the ash accumulation problem of the superheater, as shown in Figure 2. The model calculation domain is a rectangular parallelepiped with a length of 744 mm, a width of 50 mm, and a height of 104 mm.

**Figure 2** Sectional view of the computational domain model

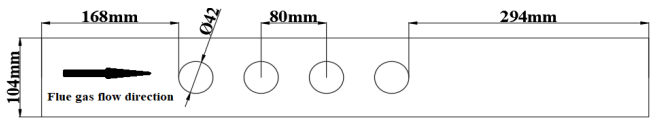


## 2.4 Numerical solution

The flow in the superheater is turbulent flow. The standard $k$-$\varepsilon$ model is stable and reliable and can meet most engineering precision. This model is used to simulate the gas phase (continuous phase). The DPM discrete phase model is used to simulate the movement of ash particles in the flue gas. The $k$-$\varepsilon$ turbulence model is calculated to obtain a convergent gas-phase flow field and then loaded into the DPM model to calculate the particle phase's particle trajectory. The discrete random walk model is used to calculate the influence of turbulent pulsation on the motion of discrete phase particles. UDF macros and C language functions are used. The library compiles the integrated growth model of the ash and then loads the UDF using the compilation mode to calculate the deposition amount of the ash. The solution process is shown in Figure 3.

Calculation method: the SIMPLE algorithm is used to calculate the gas phase flow field. The relevant model parameters and relaxation coefficients are set as the default values, and the second-order upwind discretisation is selected for the discretisation of the basic equation.

## 2.5 Simulation conditions

Simulation boundary conditions are determined by testing and reasonable assumptions. The details are as follows: after the actual measurement, the average particle size of ash is equal to 8 um, and the distribution uniformity coefficient is equal to 0.9. When ash particles in the flue gas collide with the wall surface of the heat exchange tube, it is set as an escape. The boundary conditions of flue gas inlet and outlet are set as velocity inlet and pressure outlet respectively, flue gas velocity is 5 m/s, and flue gas temperature is 603 K. The wall surface of the heat exchange tube bundle is set as a constant temperature (543 K) non-slip wall surface. The wall of the flow field parallel to the heat exchange tube bundle is set as a symmetrical wall, and the wall intersecting with the heat exchange tube bundle is set as an adiabatic non-slip wall. The gravitational acceleration is 9.8 m/s$^2$. The physical properties and operating parameters of the flue gas are shown in Table 1.

**Table 1** Physical properties and operating parameters of flue gas

| *Physical parameters* | *Value* | *Units* |
|---|---|---|
| The flue gas temperature | 603 | K |
| Mass flow inlet | 350,000 | m$^3$/h |
| The ash concentration | 60 | g/m$^3$ |
| Ash density | 2,600 | kg/m$^3$ |
| Coefficient of restitution | 0.9 | |
| Surface Poisson ratio | 0.27 | |
| Particle Poisson ratio | 0.27 | |
| Surface young's modulus | $4.92 \times 10^{10}$ | Pa |
| Particle young's modulus | $1.17 \times 10^{49}$ | Pa |

**Figure 3** The ash accumulation simulation flowchart

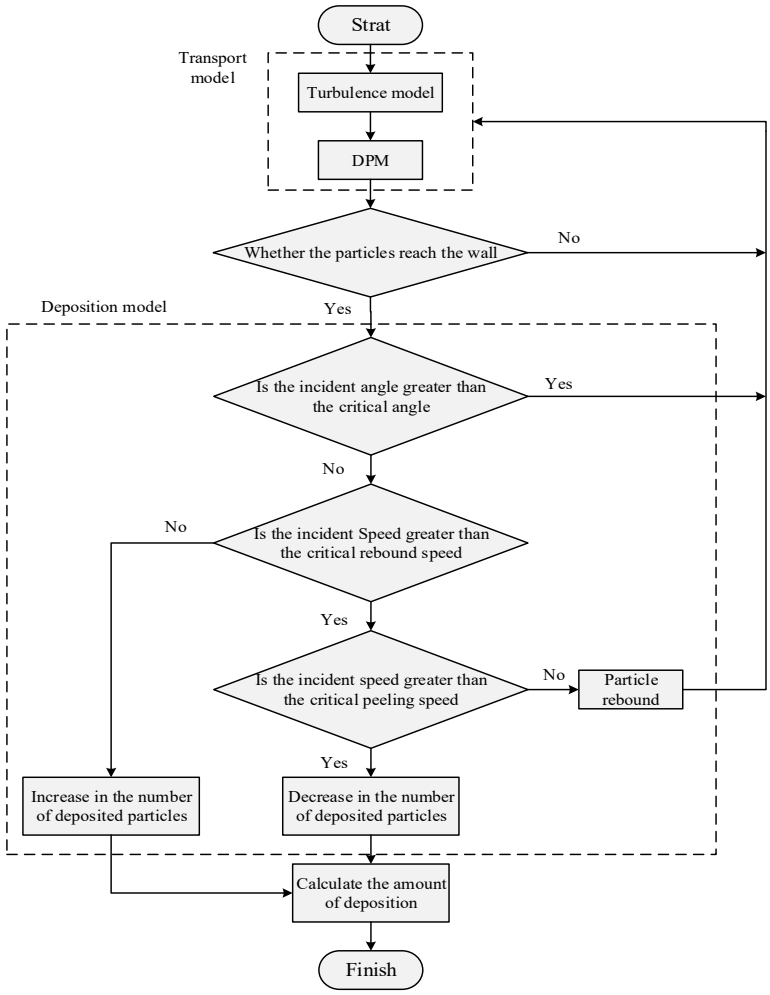


## *2.6 Computational grids*

The grid is divided by GAMBIT software. The size-function is used to divide the heat exchanger tube wall into a triangular grid. The grid near the wall surface of the heat exchange tube (including the ash deposit area and the fluid boundary layer laminar flow bottom layer) is encrypted with a grid size of 0.05 mm. The maximum mesh size in other areas is limited to 4 mm. The calculation mesh is shown in Figure 4.

**Figure 4** Superheater meshing diagram (see online version for colours)

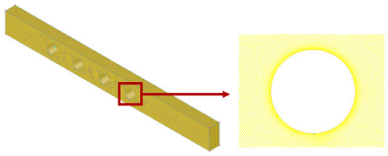

This paper uses the same meshing method and different mesh sizes to mesh the ash accumulation model. Then, the steady-state flow field simulation calculation is performed respectively. Figure 5 shows the change of the flue gas outlet temperature and the heat transfer coefficient of the heat tube surface with the number of grids. It can be seen from Figure 5 that the outlet temperature and the heat transfer coefficient of the heat tube surface have gradually remained stable after about 1.6 million. Therefore, this paper selected a grid model with a number of 1.6 million grids as the better model for the numerical simulation of fouling in the tube bundle of the SP waste heat boiler superheater.

**Figure 5** Grids independence verification calculation diagram (see online version for colours)

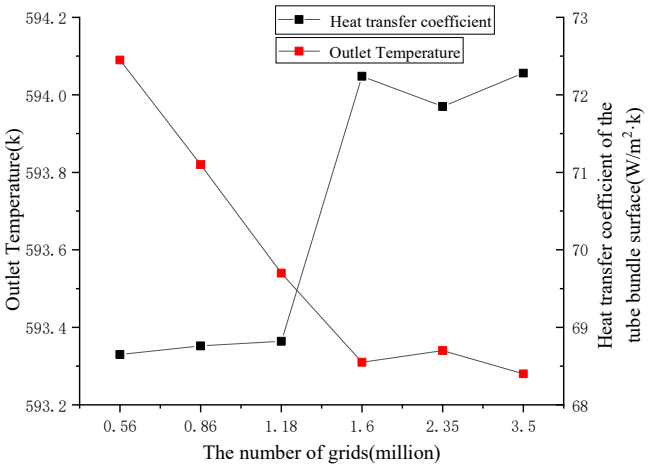

## 3 Model verification and simulation calculation results

### 3.1 Model verification

Chen Heng's ash accumulation experiment (Chen et al., 2015) analysed many physical and chemical characteristics of typical coal ash. It used the cold ash accumulation experiment platform to study the ash accumulation on the low-temperature heating surface of power station boilers. Adopt the data of Chen Heng's ash accumulation experiment as the experimental data of the comprehensive ash accumulation model verification. Chen Heng's ash accumulation experiment (the inlet flue gas velocity is 8.3 m/s, the ash concentration is 16.06 g/m$^3$) are used as the boundary conditions for the simulation calculation of the comprehensive ash accumulation growth model. The experimental results and simulation results are shown in Figure 6. It is known from Figure 6 that the experimental curve is highly similar to the simulation curve of the comprehensive ash accumulation growth model. After the deposition amount is stable, the maximum error of the two is 8.3%, less than 10%. The comprehensive ash accumulation growth model can better meet the engineering needs and calculation needs. Treating the flue gas into incompressible fluid, and the ash on the tube wall during the experiment is low-temperature loose, resulting in the incomplete collection, which should be an important reason for certain errors.

### 3.2 Ash accumulation prediction

Based on the high reliability of the Chen Baokang ash growth prediction model, and the almost complete similarity between the simulation value of the integrated ash deposition model and the sedimentation curve calculated by the Chen Baokang ash growth prediction model, this paper uses The Chen Baokang ash growth prediction model, which fits the initial simulation values of the comprehensive ash accumulation model to obtain a comprehensive ash accumulation prediction model as shown in equation (26):

$$m_f = m_f^*[1-\exp(-t/\tau)] \tag{26}$$

In equation (26): $t$ is time; $m_f$ is the average ash deposit; $\tau$ is the ash accumulation time constant, which refers to the time required for the ash deposition to reach a steady-state; $m_f^*$ is the maximum deposition amount, which refers to the final stable ash deposit amount is achieved. The maximum deposition amount and the ash accumulation time constant are obtained by fitting the initial simulation values.

Figure 7 and Figure 8 show the calculation results of the ash accumulation prediction model based on the first 120 s of the ash accumulation simulation value and the comparison of the 500 s simulation results when the flue gas velocity is 5 m/s and 7 m/s (the ash concentration is 30 g/m$^3$). It is known from the two figures that the error between the two is tiny, and the difference gradually increases with time and finally tends to be fixed. When the flue gas velocity is 5 m/s, the error between the two is 6.6%. When the flue gas velocity is 7 m/s, the error between the two is 4.2%. The errors of the above two conditions are lower than the engineering tolerance. Therefore, the fitting prediction model can better predict the deposition of ash in the subsequent time.

**Figure 6** Comparison of experimental data and simulation results (see online version for colours)

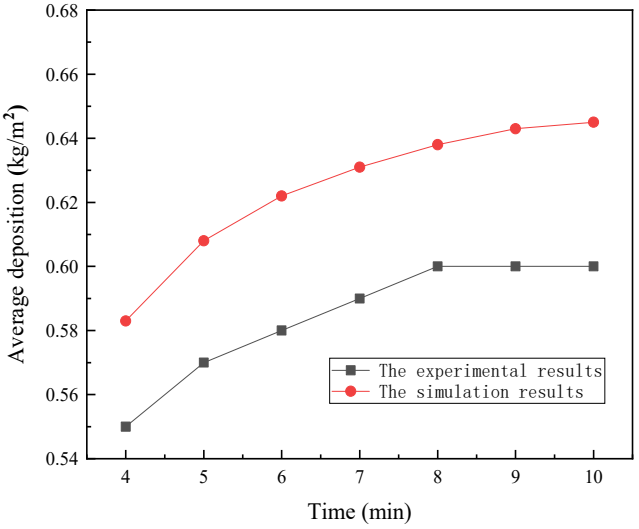


**Figure 7** Comparison of simulation results and fitting results (the inlet flue gas velocity is 5 m/s, the ash concentration is 30 g/m$^3$) (see online version for colours)

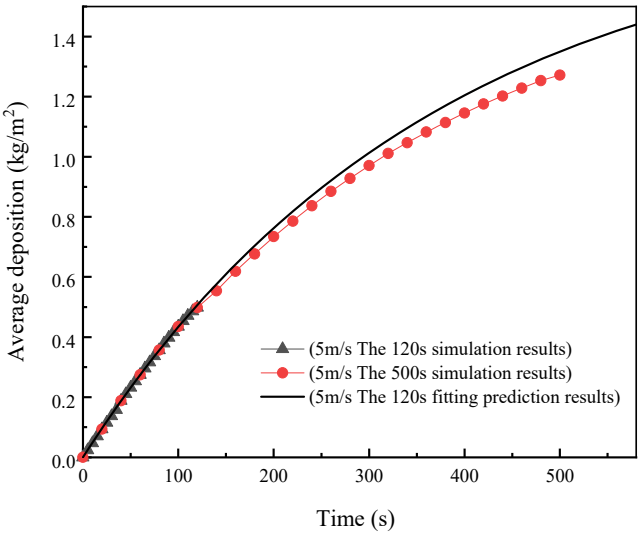


### 3.3 Effect of flue gas velocity on ash accumulation

Four simulation cases in which flue gas velocity is 3 m/s, 5 m/s, 7 m/s, 9 m/s are performed to investigate the effect of flue gas velocity on ash accumulation. The ash concentration in the flue gas of the four simulation cases is 30 g/m$^3$. The velocity distribution of the vertical section of the tube bundle axis at different inlet velocities is shown in Figure 9.

**Figure 8** Comparison of simulation results and fitting results (the inlet flue gas velocity is 7 m/s, the ash concentration is 30 g/m$^3$) (see online version for colours)

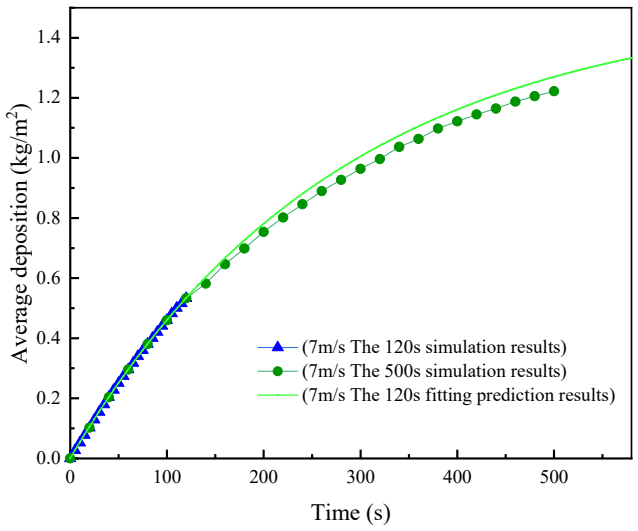


**Figure 9** Velocity distribution of the vertical section of the tube bundle axis at different velocities (flue gas flows from left to right) (see online version for colours)

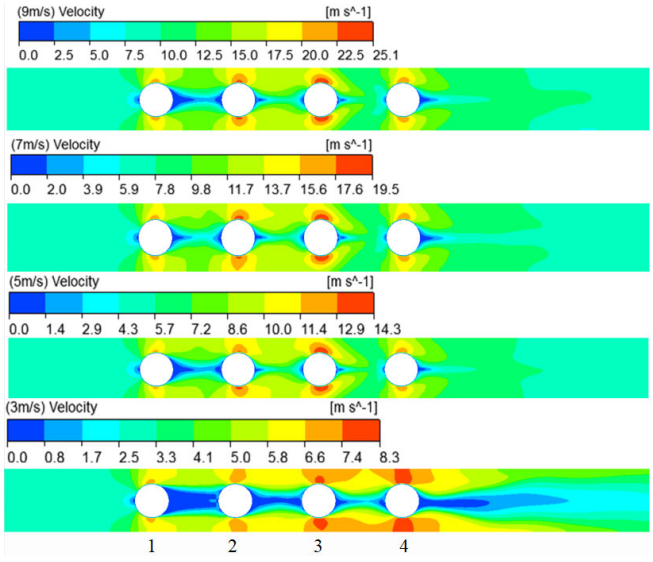


It can be seen from Figure 9 that as the flue gas velocity at the inlet of the superheater increases, the highest velocity region in the calculation domain always appears on the side of the heat exchange tubes, but the position moves forward from the vicinity of the third and fourth rows of tube walls to the vicinity of the second and third rows of tube walls, and the maximum speed in the calculation domain increases from 8.3 m/s to 25 m/s. The rigidity of the flue gas after flowing through the heat exchange tube increases, the filling area increases, and the area of the low-velocity zone decreases.

The distribution of ash deposition on the front projection of the heat exchange tubes at different velocities is shown in Figure 10. It can be seen that the ash accumulation mainly occurs in the central area of the tube walls and is symmetrically distributed along the flue gas flow direction; the ash accumulation area of the first row of heat exchange tubes is elongated, and the ash accumulation area of the last three rows of heat exchange tubes is circular; the second row is the least dense; the third row is lighter than the fourth row; the fourth row is the most severe compared to the first three rows. In combination with Figure 9, it can be concluded that the velocity of the flue gas stream superheater tube bundle changes as the flow cross-sectional area changes. When the flue gas flows through the two sides of the tubes, the velocity is the highest; when the flue gas flows past the central section of the tube area, the flow velocity is the smallest. When the flue gas flows through the heat exchange tubes, eddy current is generated due to the flow around the cylinder. When flowing through the first row, the eddy current level is low, and the ash accumulation area is elongated; when flowing through the last three rows, the eddy current is formed by the flow around the first row. The ash accumulation area on the tube walls is circular. With the increase of flue gas velocity, the ash accumulation area of the first row of heat exchange tubes increased, and the degree of ash accumulation increased; the size and sedimentation degree of the second row of ash accumulation areas did not change significantly; when the area of the third and fourth rows of ash accumulation is slightly enlarged, the two symmetric accumulation areas gradually merge; after the smoke velocity is more than 7 m/s, the degree of ash accumulation gradually decreases.

**Figure 10** Distribution of ash deposition on the front projection of the heat exchange tubes at different velocities (see online version for colours)

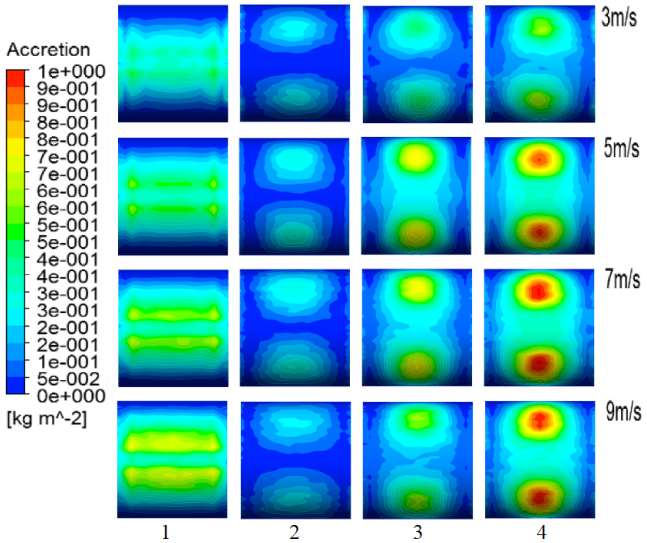


The effect of the inlet velocity calculated by the fitting prediction model on the average deposition of the heat exchange tube bundle is shown in Figure 11. It can be seen that as the inlet velocity of the flue gas increases, the deposition rate increases as the total amount of ash carried by the flue gas increases. In the low-speed stage, the deposition amount and the maximum deposition amount increase with the increase of the flue gas inlet velocity; when the flue gas velocity exceeds the critical stripping speed, the initial deposition is dominant, the initial

deposition increases with the increase of the velocity. The exfoliation dominates later, the maximum deposition amount decreases as the flue gas velocity increases.

**Figure 11** Effect of flue gas velocity on the average deposition of heat transfer tube bundles (see online version for colours)

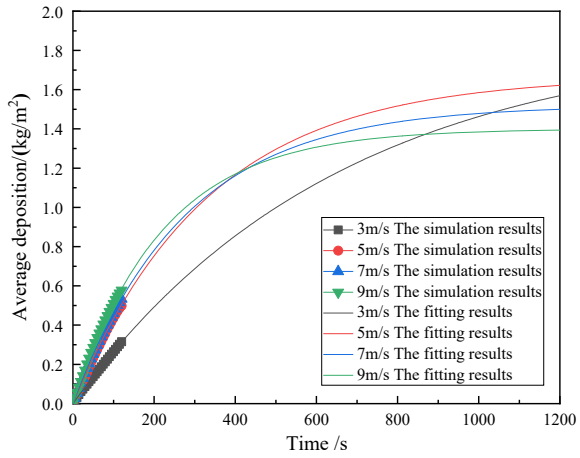


**Figure 12** Effect of flue gas velocity on maximum ash deposition amount and ash accumulation time constant (see online version for colours)

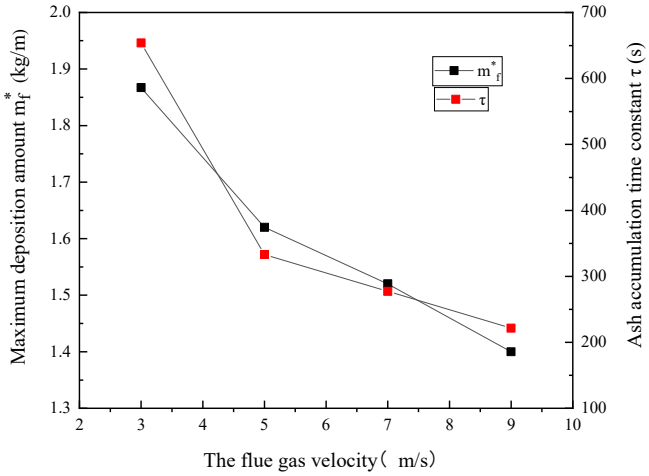


According to the analysis of equation (26), the deposition rate of ash is determined by the ash accumulation time constant $\tau$ and the maximum deposition amount $m_f^*$. The larger the ash accumulation time constant $\tau$ is, the smaller the deposition rate is. The larger the deposition amount $m_f^*$ is, the larger the deposition rate is. The relationship between the ash accumulation time constant $\tau$ and the maximum deposition amount $m_f^*$ as a function of the inlet flue gas velocity is shown in Figure 12. It can be seen from Figure 12 that the ash accumulation time constant $\tau$ and the maximum deposition amount $m_f^*$ are negatively correlated with the flue gas velocity. With the flue gas velocity increasing from 3 m/s to 9 m/s. The deposition amount $m_f^*$ decreased from 1.88 kg/m$^2$ to 1.41 kg/m$^2$, a drop of nearly 25%, and the ash accumulation time constant $\tau$ decreased from 670 s to 220 s, a drop of nearly 67%. The ash accumulation time constant $\tau$ and the maximum deposition amount $m_f^*$ are inversely proportional to the inlet velocity of flue gas. It is easy to conclude that when the inlet flue gas velocity increases to the critical stripping velocity, as the flue gas inlet velocity increases, due to the stripping effect of the deposited particles increases, the maximum deposition amount gradually decreases. Due to the acceleration of deposition the accumulation time is gradually reduced. When the inlet flue gas velocity rises to about 5 m/s, the effect of the stripping velocity on the sediment rises to a dominant position, the deposition time constant curve turns, and the dropping speed of the time constant gradually slows down.

### *3.4 Effect of ash concentration on ash accumulation*

To investigating the effect of ash concentration of flue gas on ash accumulation, five simulation cases are performed. The ash concentration in each case is 30 g/m$^3$, 60 g/m$^3$, 90 g/m$^3$, 120 g/m$^3$, 150 g/m$^3$, respectively. The flue gas velocity is kept at 5 m/s. Figure 13 shows the distribution of ash deposition on the windward side of the heat exchange tube at different ash concentrations at 120 s. It can be seen that the deposition area and deposition amount of ash on the tube walls increase with the increase of the ash concentration of the flue gas.

**Figure 13** Distribution of ash deposition on the front projection of the heat exchange tubes at different ash concentrations (see online version for colours)

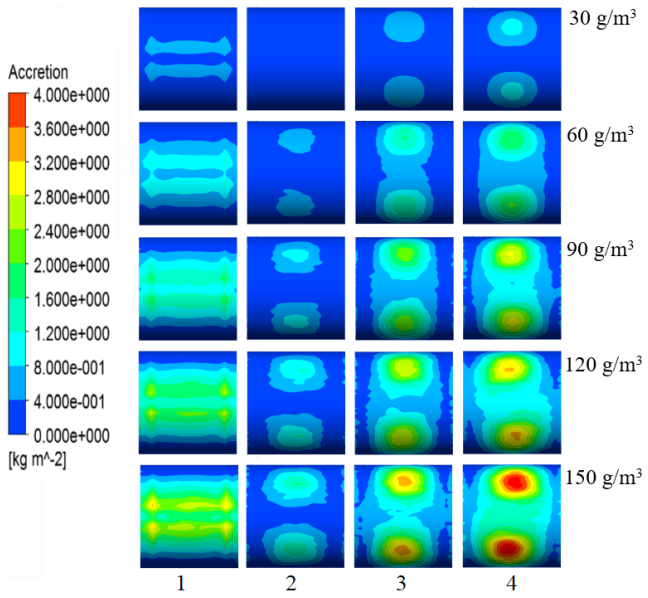


The effect of the inlet ash concentration calculated by the fitting prediction model on the average deposition of the heat exchange tubes is shown in Figure 14.

It can be seen from Figure 14 that the deposition rate increases as the ash concentration increases. In the lower concentration region, the deposition rate increases with the increase of ash concentration. When the concentration is higher than 120 g/m$^3$, the growth rate decreases gradually, and the deposition rate tends to be stable. This is because

that under high ash concentration conditions, the action of the fluid micelles plays a dominant role in the deposition. As the ash concentration increases, the deposition rate of particles increases, and the reverse velocity of the fluid increases with deposition, which hinders the increase of deposition rate, slows the deposition rate of particles and eventually stabilises.

**Figure 14** Effect of ash concentration on the average deposition of heat exchange tubes (see online version for colours)

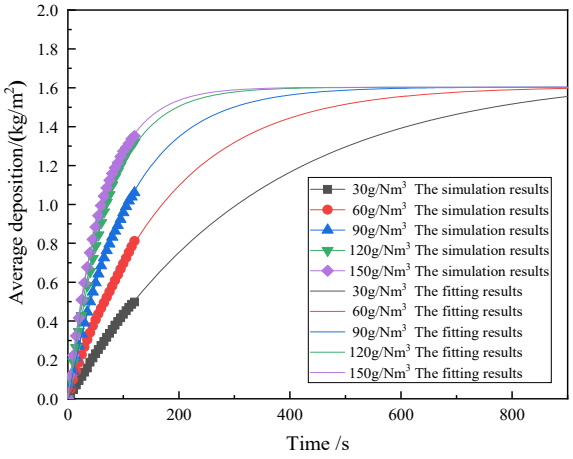


**Figure 15** Effect of ash concentration on maximum ash deposition amount and ash accumulation time constant

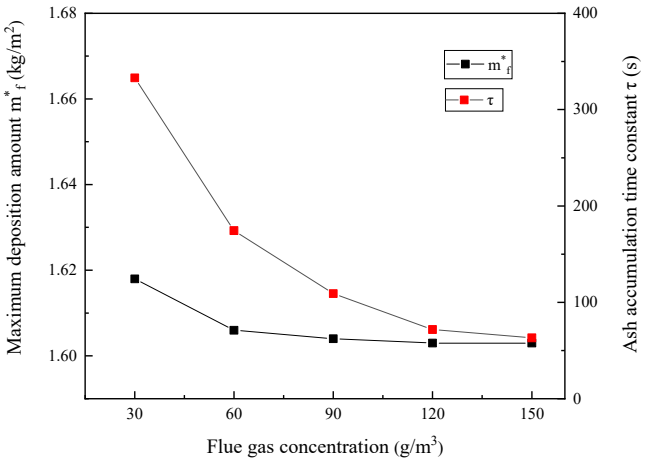


The effect of the ash concentration calculated by the fitting prediction model on the maximum deposition amount $m_f^*$ and the ash accumulation time constant $\tau$ is shown in Figure 15. Because the flow field conditions in the computational domain are basically the same and the particle motion states are also basically the same, the maximum deposition amount $m_f^*$ is almost kept constant at different ash concentrations. The maximum deviation of maximum deposition amount $m_f^*$ among the five cases with different concentrations is less than 0.02 kg/m$^2$, and the relative deviation is less than 2%. The ash accumulation time constant $\tau$ decreases as the ash concentration of the flue gas increases. Based on the above studies, it is easy to conclude that the ash concentration only affects the time when the deposition rate and the deposition-stripping reach equilibrium and has little effect on the maximum deposition amount.

### *3.5 Effect of different tube layout angles of oval tubes on ash accumulation and comparison with round tubes*

The circumference of the oval tube and the circular tube are both 131.95 mm. According to the research results with the best anti-ash accumulation effect is when the length-diameter ratio of the oval tube is 3:1 (Lou, 1995), so the long diameter of the oval tube is 59.5 mm, and the short diameter is 20 mm. To investigate the effect of oval tube angle on ash accumulation, five simulation cases in which the oval tube angle in each case is 0°, 25°, 45°, 65°, 90° are performed. The flue gas velocity of the five simulation cases is kept at 5 m/s, and the ash concentration of the flue gas is 30 g/m$^3$. The distribution of the ash deposition of the oval tube in the windward area is shown in Figure 16.

**Figure 16** Distribution of ash deposition on the front projection of the oval tubes with different layout angles

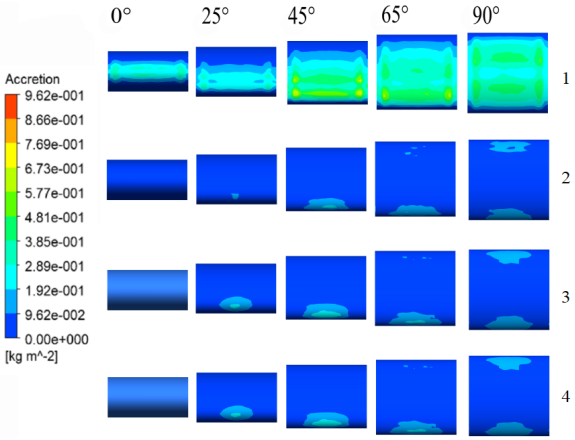


**Figure 17** Effect of oval tube layout angle on the average deposition of superheater (see online version for colours)

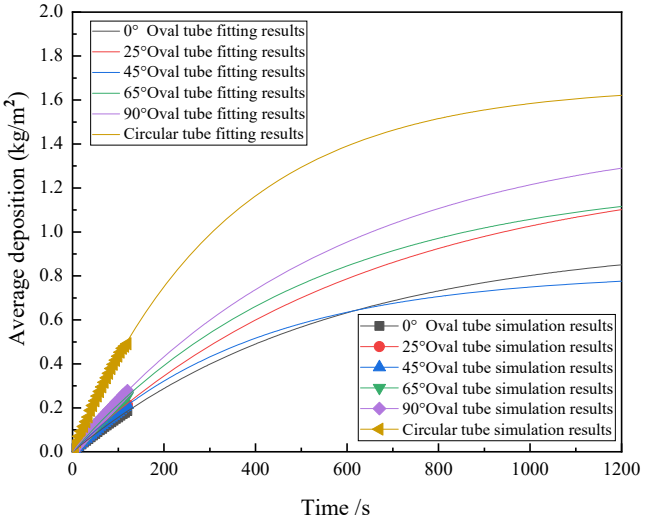

It can be seen from Figure 17 that the ash accumulation on the windward side of the oval tube mainly occurs in the position of the first row of heat exchange tubes. And ash accumulation area of the windward area increases with the increasing layout angle of the oval tube. The central area of the windward surface of the first row of oval tubes blocks the airflow due to the wall surface so that the flue gas flow rebounds and disperses to the two sides, creating a low-speed region. Its area gradually increases as the oval tube layout angle increases. On the first row, the deposition area is getting larger and larger; the deposition degree gradually increase. Although the deposition area of the second, third and fourth rows is gradually increased, the overall deposition amount is small and basically the same.

**Figure 18** Effect of oval tube layout angle on maximum ash deposition and ash time constant (see online version for colours)

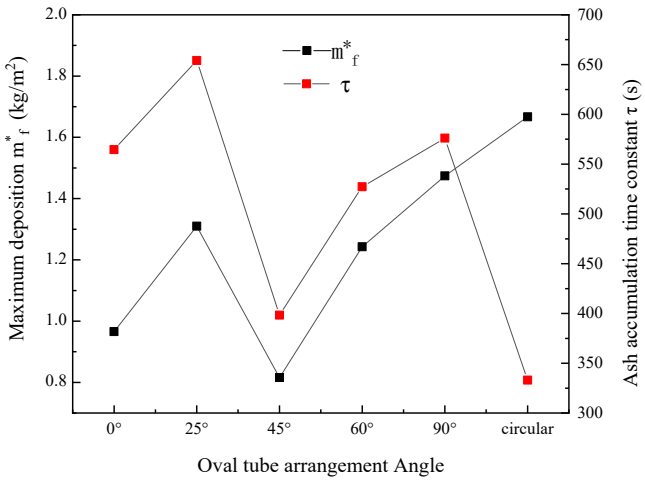


Figure 17 shows the effect of the oval tube layout angle calculated by the fitting prediction model on the average deposition of the superheater. Figure 18 shows the effect of the oval tube layout angle calculated by the fitting prediction model on the maximum deposition amount $m_f^*$ and the ash accumulation time constant $\tau$ of the oval tube superheater. It can be seen that the maximum ash deposit of the round tube is larger than the maximum ash deposit of the oval tube by Figure 17 and Figure 18. The ash accumulation time constant of the round tube is the smallest. For oval tubes, the ash deposition at 0° and 45° is the smallest; the deposition of ash at 25° and 65° is equivalent; the deposition at 90° is the largest. A comprehensive comparison shows that the average ash accumulation of the oval tube at 45° is the smallest, and the ash deposition speed is comparable to that of the round tube.

## 4 Conclusions

1 A comprehensive ash accumulation model is established, and the reliability of this model is validated.

2 The fitting prediction model based on the initial simulation value of the comprehensive ash accumulation model can better predict the growth of ash accumulation in the later period.

3 As the flue gas velocity and ash concentration increase, the deposition rate of the ash increases, and the time for the ash deposition to reach equilibrium (the ash accumulation time constant) decreases; the increase of the ash concentration has little effect on the ash deposit; the maximum deposition of ash is gradually reduced as the inlet velocity of the flue gas increases.

4 Through simulation, to alleviate the superheater ash accumulation in the actual operation of the boiler, the flue gas velocity recommended in this paper is 5 m/s; the ash concentration in the smoke is 60 g/m$^3$. In addition, it is recommended to design the superheater tube structure into an oval, and the oval tube layout angle is 45°.

## References

Abd-Elhady, M.S., Rindt, C.C.M., Wijers, J.G. and Van Steenhoven, A.A. (2006) 'Modeling the impaction of a micron particle with a powdery layer', *Powder Technology*, Vol. 168, No. 3, pp.111–124.

Amiri, A. and Vaseghi, M.R. (2015) 'Waste heat recovery power generation systems for cement production process', *IEEE Transactions on Industry Applications*, Vol. 51, No. 1, pp.13–19.

Chen, B.K., Yan, W.P., Zhu, Y.D., Gao, Z.Y. and Liang, X.J. (2004) 'Study on prediction model of fouling layer growth on convective heating surface of coal-fired power station boiler', *Journal of North China Electric Power University (Science edition)*, Vol. 31, No. 2, pp.21–35.

Chen, H., Wang, Y.G., Zhao, Q.X., Chen, Z.Y. and Zhang, J.F. (2015) 'Experimental investigation of ash deposition on low temperature heating surfaces in a coal-fired boiler', *Proceedings of the CSEE*, Vol. 35, No. S1, pp.118–124.

Fang, Q., Wang, H. and Wei, Y. (2010) 'Numerical simulations of the slagging characteristics in a down fired, pulverized-coal boiler furnace', *Fuel Processing Technology*, Vol. 91, No. 1, pp.88–96.

Gu, L., Yuan, W.D., Tang, C. and He, Q.H. (2017) 'Influence factors and prevention methods of ash accumulation in pure low temperature waste heat boiler in cement kiln', *Metallurgical Collections*, Vol. 2017, No. 1, pp.93–95.

Han, H., He, Y.L, Tao, W.Q. and Li, Y.S. (2014) 'A parameter study of tube bundle heat exchangers for fouling rate reduction', *International Journal of Heat and Mass Transfer*, Vol. 72, pp.210–221.

Harding, N.S. and O'Connor, D.C. (2007) 'Ash deposition impacts in the power industry', *Fuel Processing Technology*, Vol. 88, Nos. 11–12, pp.1082–1093.

Johnson, K.L., Kendall, K. and Roberts, A.D. (1971) 'Surface energy and the contact of elastic solids', *Proceedings of the Royal Society of London. Series A, Mathematical and Physical Sciences (1934-1990)*, Vol. 324, No. 1558.

Johnson, K.L. (1985) *Contact Mechanics*, Cambridge University Press, Cambridge, UK.

Kong, X.Z. (2009) 'The contribution of waste heat power generation technology to energy conservation and emission reduction in China's cement industry', *China International Cement Summit*, Beijing.

Lin, J.S. and Tsai, C.J. (2003) 'Thermophoretic deposition efficiency in a cylindrical tube taking into account developing flow at the entrance region', Vol. 34, No. 5, pp.569–583.

Lou, X.R. (1995) *Study on Beam Resistance and Heat Transfer Performance of Elliptic Shaped Tube*, Master, South China University of Technology, China.

Miao, H., Yin, H., Shang, Y., Chi, X. and Mu, L. (2022) 'Numerical prediction on deposition growth and heat transfer characteristics burning high-sodium pulverized coal', *Fuel*, Vol. 309, pp.122–135.

Mindlin, R.D. (1949) 'Compliance of elastic bodies in contact', *Journal of Applied Mechanics*, Vol. 16, pp.259–268.

Mu, L., Miao, H., Zhao, C., Zhai, Z., Shang, Y. and Yin, H. (2021) 'Dynamic CFD modeling evaluation of ash deposition behavior and morphology evolution with different tube arrangements', *Powder Technology*, Vol. 379, pp.279–295.

Pérez, M.G., Vakkilainen, E. and Hyppänen, T. (2016) 'Unsteady CFD analysis of kraft recovery boiler fly-ash trajectories, sticking efficiencies and deposition rates with a mechanistic particle rebound-stick model', *Fuel*, Vol. 181, pp.408–420.

Ren, C., Jiang, M., Zou, L., Li, X.Q. and Wei, Y.X. (2014) 'Study on establishment of emission control level of air pollutants in cement industry', *Environmental Science*, Vol. 2014, No. 9, pp.3632–3638.

Si, H.J. and Fan, G.Q. (2015) 'Effect of ash accumulation on operation of waste heat boiler', *National Conference on Energy and Thermal Engineering*, Dalian.

Tang, S.Z., He, Y.L., Wang, F.L. and Tao, Y.B. (2018) 'Parametric study on fouling mechanism and heat transfer characteristics of tube bundle heat exchangers for reducing fouling considering the deposition and removal mechanisms', *Fuel*, Vol. 211, pp.301–311.

Thornton, C. and Ning, Z. (1998) 'A theoretical model for the stick/bounce behaviour of adhesive, elastic-plastic spheres', *Powder Technology*, Vol. 99, No. 2, pp.154–162.

Yang, X., Ingham, D., Ma, L., Zhou, H. and Pourkashanian, M. (2017) 'Understanding the ash deposition formation in Zhundong lignite combustion through dynamic CFD modelling analysis', *Fuel*, Vol. 194, pp.533–543.

Ye, F.X., Ding, H.L. and Pan, W.G. (2018) 'Numerical study on heat transfer, wear and fouling performance of circular tube bundle and elliptical tube bundle', *Proceedings of the CSEE*, Vol. 38, No. 11, pp.3289–3294.

Zbogar, A., Frandsen, F., Jensen, P.A. and Glarborg, P. (2009) 'Shedding of ash deposits', *Progress in Energy & Combustion Science*, Vol. 35, No. 1, pp.31–56.

Zhang, D.J., Wang, J.F., Wang, J.Q., Dai, Y.P. and Peng, Y. (2009) 'Analysis and optimization of waste heat power generation technology of cement kiln', *Journal of Chinese Society of Power Engineering*, Vol. 29, No. 9, pp.885–890.

Zhang, H., Zhao, H., Li, Z. and Hu, E. (2018) 'Optimization potentials for the waste heat recovery of a gas-steam combined cycle power plant based on absorption heat pump', *Journal of Thermal Science*, 2019, Vol. 28, pp.283–293.

## Nomenclature

| | |
|---|---|
| *Latin letters* | |
| $a$ | Contact radius |
| $E^*$ | Effective modulus |
| flue gas | Flue gas |
| $F_t$ | Adhesion force |
| $F_t$ | Tangential force |
| $G^*$ | Effective shear modulus |
| $k_t$ | The tangential stiffness |
| $m$ | Grain quality |
| $m^*$ | Effective collision quality |
| $m_f^*$ | Maximum deposition |
| $P_c$ | Pressure |
| $Q_A$ | Adhesion energy |
| $Q_{in}$ | Normal impact energy |
| $Q_{it}$ | Tangential impact energy |
| $Q_p$ | Energy loss |
| $R^*$ | Effective contact radius |
| SP | Suspension preheater |
| $t$ | Time |
| UDF | User-defined function |
| $V_i$ | Incidence velocity |
| $V_{in}$ | Normal velocity |
| $V_s$ | Critical rebound velocity |
| $V_t$ | Bounce velocity |
| $V_t$ | Tangential velocity |
| $V_y$ | Critical stripping velocity |
| $W_s$ | Extra rebound work |
| *Greek letters* | |
| $\alpha$ | Relative approach |
| $\Gamma$ | Surface energy |
| $\Delta t$ | Collision contact time |
| $Q_\varepsilon$ | Elastic potential energy |
| $\theta'$ | Angle of incidence |
| $\theta_{ca}$ | Critical incident angle |
| $\mu^*$ | Friction coefficient |
| $\tau$ | Ash time constant |